A clamped-beam bending test method for the flexural behaviour of uncured metal-CFRP laminates

Liu, Shichen; Sinke, Jos

DOI
10.1177/00219983251351404

Publication date
2025

Document Version
Final published version

Published in
Journal of Composite Materials

Citation (APA)
Liu, S., & Sinke, J. (2025). A clamped-beam bending test method for the flexural behaviour of uncured metal-CFRP laminates. *Journal of Composite Materials*, *59*(30), 3411-3430. Article 00219983251351404. https://doi.org/10.1177/00219983251351404

Original Manuscript

JOURNAL OF COMPOSITE MATERIALS

Journal of Composite Materials
2025, Vol. 0(0) 1–20

DOI: 10.1177/00219983251351404
journals.sagepub.com/home/jcm
Sage

A clamped-beam bending test method for the flexural behaviour of uncured metal-CFRP laminates

Shichen Liu[1,2] and Jos Sinke[2]

Abstract

This paper examines the flexural behaviour of uncured metal-carbon fibre reinforced polymer (CFRP) laminates when subjected to clamped-beam bending conditions. The test method was developed to assess how clamping affects the ratio between stretching and drawing during a proposed press forming process. The study compared the effects of variations in metal composition, layup, fibre orientation, and processing temperature on bending force, spring-back depth, and sliding length. The results revealed that increasing clamping pressure from 0 bar to 6 bar for aluminium-based hybrid materials with a 2/1 layup decreased the interlaminar sliding length by 3%, resulting in a rise in plastic strain in the metal layer from 2.55% to 15.22% and a reduction in spring-back by 10%. Additionally, the maximum bending forces for the uncured 2/1 metal-CFRP laminates were found to be slightly higher than twice that of the corresponding single-layer metal sheets. The processing temperature, ranging from room temperature to 110°C, was also shown to affect the bendability of the laminate, particularly at a clamping pressure of 0 bar. Furthermore, both numerical and experimental results demonstrated a strong correlation at room temperature across various clamping pressures for the hybrid materials studied.

Keywords

Metal-CFRP laminates, clamping pressure, bending force, spring-back depth, plastic deformation

Introduction

In recent years, the development of new lightweight materials with excellent mechanical properties has attracted significant interest from researchers in the field of aircraft manufacturing. Metal-composite laminates, also known as fibre-metal laminates (FMLs), are a prominent example, fabricated by alternating layers of thin metal alloy sheets and fibre-reinforced polymers.[1,2] These hybrid laminates combine the advantages of metallic materials and fibre-reinforced matrix systems, offering notable benefits such as significant weight reduction, high specific strength and stiffness, along with superior fatigue and corrosion resistance.[3–5] As a hybrid material, metal-composite laminates feature multiple interfaces, including fibre-metal, fibre-matrix, and matrix-metal interfaces. However, these interfaces are prone to delamination, particularly in the uncured state when subjected to temperature fluctuations or mechanical loads such as bending and impact, due to the disparate physical and mechanical properties of the metal and composite layer. However, these interfaces are prone to delamination, particularly in the uncured state when subjected to temperature fluctuations or mechanical loads such as bending and impact, due to the disparate physical and mechanical properties of the metal and composite layer.[6,7] Consequently, the manufacturing process for uncured metal-composite laminates presents challenges, as it requires multiple forming and curing stages involving complex deformation and failure mechanisms.[8–10]

To enhance the manufacturability of these hybrid materials, we propose an integral forming and curing cycle (Figure 1), which integrates preheating, press forming, and curing stages. During preheating, time and temperature are meticulously controlled to reduce resin viscosity, thereby enhancing inter-ply sliding at metal-prepreg interfaces and intra-ply shear within the prepregs.[11–14] This approach

[1]School of Aerospace Engineering, Xiamen University, Xiamen, PR China
[2]Faculty of Aerospace Engineering, Delft University of Technology, Delft, The Netherlands

Corresponding author:
Shichen Liu, School of Aerospace Engineering, Xiamen University, No. 4221, Xiangan Road, Xiamen 361005, PR China.
Email: liusc94@xmu.edu.cn

Data Availability Statement included at the end of the article

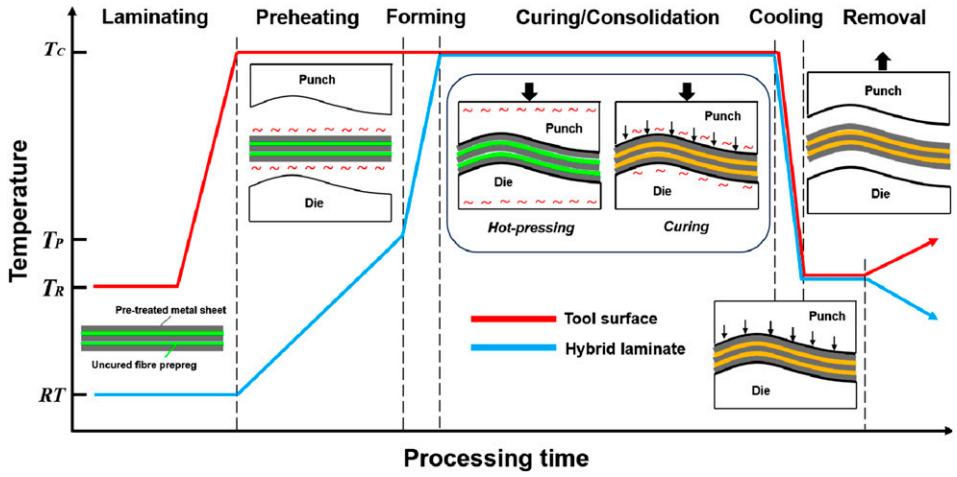

Figure 1. Processing temperature-time profile of the tool surface and hybrid laminate in an integral forming and curing cycle.

eliminates the need for additional steps, such as unloading and reloading in a separate low-pressure curing system, resulting in time and cost savings.[15,16] Furthermore, the process improves interlaminar bonding, making it particularly advantageous for small- to medium-sized components with complex geometries.[17,18] The press forming of such laminates involves a combination of bending, stretching, and drawing, leading to multi-axial in-plane and out-of-plane deformations. Thus, this research focuses on characterizing the flexural properties of individual layers and the simultaneous bending behaviour at metal-composite interfaces.

Bending is a widely used manufacturing process for producing V-shaped, U-shaped, or channel-shaped parts along a straight axis in ductile materials, primarily metal sheets. Among the methods for characterizing bending behaviour, the three-point bending test is the most common, employing a specified fixture on a universal testing machine to measure flexural modulus and bending stress-strain response.[19–21] The four-point bending test is similar, but the central section of the beam between the two load-bearing points experiences constant stress without shear. Both methods offer advantages such as simple sample geometries and compatibility with as-fabricated materials. However, the four-point bending test has limitations, including a complex stress-strain distribution through the sample.[22] While these methods are also applied to fibre-reinforced composites, many studies have historically overlooked bending behaviour due to the relatively low bending stiffness compared to in-plane shear/tension stiffness. However, recent research has highlighted the critical role of bending stiffness in preventing wrinkling during forming.[23–25]

To address this, various test methods have been developed for fibre-reinforced composites. Figure 2 illustrates three primary bending test setups for carbon fibre-reinforced polymers (CFRPs), incorporating temperature control. The cantilever test fixes one end while leaving the other free, resulting in a free radius after bending. Liang et al[26] enhanced the method by adding an environmental chamber to study temperature effects on bending stiffness. However, the influence of the specimen's weight remains a limitation, which could be mitigated by a vertical cantilever design. The Kawabata-based approach (Figure 2(b)) was developed to characterize bending behaviour in continuously fibre-reinforced composites, whether unidirectional (UD) or woven. This method measures bending moment by imposing a constant radius on the specimen through clamp rotation.[27] Sachs et.al[28] further refined this approach by integrating a rheometer and environmental chamber to evaluate rate- and temperature-dependent bending behaviour of UD tapes. Their results confirmed the suitability of the method for large-curvature deformation analysis. The Vee-bending test (Figure 2(c)), adapted from the three-point bending setup, was designed to evaluate the bending behaviour of CFRP materials. Subsequent improvements introduced geometric supports to control specimen deformation (Figure 2(d) and (e)), with the latter requiring clamps on the flanges for equilibrium.[29] Despite its ability to account for test speed and temperature effects, the fixture can become unstable near the thermoplastic resin's melting point.[30] Therefore, this study aims to develop a robust test method for accurately measuring the flexural behaviour of uncured fibre-reinforced composites, with emphasis on bending stiffness.

Existing literature primarily focuses on the bending behaviour of cured metal-composite laminates, particularly using short-beam three-point bending tests ($L/h < 10$) to evaluate interlaminar shear strength (ILSS). For example, Ostapiuk et al[31] analysed the bending and failure behaviour of glass- and carbon-fibre-reinforced laminates, noting that fibre strain/stress relationships, metal layer thickness, and

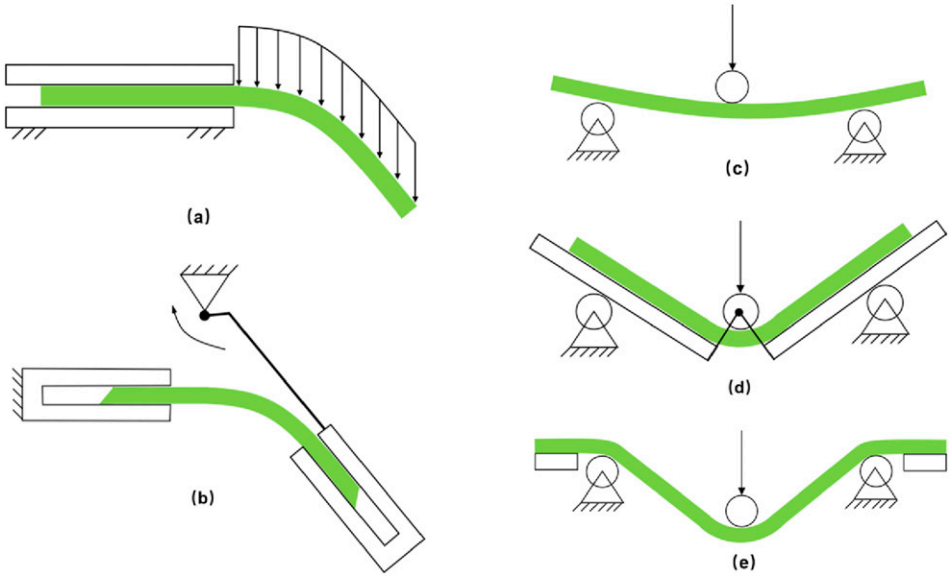

Figure 2. Setups for the characterisation of bending behaviour for fibre reinforced composites: (a) Cantilever test based, (b) Kawabata test based and (c)–(e) Vee-bending test based methods.

fibre orientation are critical factors. Liu et al[32] studied interlaminar failure in Glare laminates, finding that layup configuration significantly affects load-deflection responses and failure modes. Li et al[33] investigated bending failure mechanisms in Glare laminates with varying stacking sequences, observing that bending modulus decreases with layer count, while bending strength trends differ for UD and cross-ply laminates. Hu et al[34] combined experimental and numerical methods to characterize Al/CFRP laminates, concluding that higher metal volume fractions reduce bending modulus and strength, with CFRP playing a dominant role. Despite these advances, there is a lack of research on long-beam bending tests (L/h > 100) for uncured epoxy-based laminates, as well as the influence of metal sheets and clamping pressure on stretch-to-draw ratios during forming. Additionally, numerical and experimental methods for selecting material compositions, laminate structures, and processing parameters remain underexplored. Addressing these gaps is essential for understanding the flexural behaviour of uncured metal-CFRP laminates.

This study aims to characterize the flexural behaviour of uncured metal-CFRP laminates using a clamped-beam bending test. We examine laminates comprising aluminium alloy, stainless-steel, and CFRP layers to assess the effects of metal composition, laminate layup, fibre orientation, and processing temperature under varying clamping pressures. A custom clamped-beam test setup was designed to simulate actual forming conditions and accommodate uncured laminate characteristics. Experimental tests and finite element modelling are employed to validate load-displacement responses, bendability metrics (e.g., spring-back depth, length reduction), and the shape of the final part. The findings will advance the understanding of flexural behaviour and optimize material selection and process parameters for hot-pressing uncured metal-CFRP laminates.

Material and methods

Material preparation

The metal-composite laminates investigated in this study consist of aluminium alloy 2024-T3 sheets, stainless-steel 304L sheets, and T300 carbon fiber-MTC510 unidirectional (UD) prepregs. Prior to lamination, the aluminium alloy surfaces were anodized using phosphoric acid, and both metal sheets (0.5 mm thick) were cleaned with acetone.[1,2] For the composite layers, two cross-ply UD prepreg configurations of 0°/90° and 45°/−45° with a nominal total thickness of 0.3 mm were selected. Besides, each ply had a fibre volume fraction of 60%, and the epoxy-based prepregs exhibited a significant viscosity reduction when heated from room temperature (23°C) to 110°C at a rate of 2°C/min.[35] The mechanical properties of the materials are summarized in Table 1, with the assumption that metal properties remain stable within the studied temperature range.[36,37] The elastic modulus, shear modulus, and ultimate strength of the UD prepregs are reported for both 0° and 90° fibre orientations. In all laminates, the metal rolling direction and 0° fibre orientation were aligned parallel to the bending axis.

Table 1. Mechanical properties of the material compositions in hybrid laminates.[35-37]

Materials	Density (g/cm^3)	Elastic modulus (GPa)	Shear modulus (GPa)	Yield strength (MPa)	Poisson's ratio	Ultimate strength (MPa)	Shear strength (MPa)	Elongation at break (%)
Aluminium alloy 2023-T3	2.7	71	28	320	0.33	480	283	16.2
Stainless-steel 304L	8.0	200	77	210	0.30	574	378	45.6
UD carbon fibre prepreg-MTC510	1.5	119.3/8.2	3.6/2.0	-	0.34	2282/54	99.0	1.3

Concept design

The clamped-beam bending test concept originated from the integral forming and curing cycle proposed for press forming (Figure 1). While traditional three-point bending accounts for material compositions, laminate structures, and preheat temperatures, it neglects critical factor like forming pressure on flange region, which are essential for material flow and wrinkling control. To address this limitation, a clamped-beam bending test was developed, combining principles from three-point and fixed-beam bending. The schematic graph and dimensions of the clamped-beam bending concept are shown in Figure 3. A 300 × 50 mm laminate is positioned symmetrically on supports and clamped by two 50 × 50 mm blocks. Then a 10 mm diameter punch applies a vertical displacement along the laminate centreline. To ensure uniform clamping pressure, a double-acting pneumatic cylinder (FESTO ADN-50-10-A-P-S6) was employed (Figure 4). This system operates in both extension and retraction strokes, meeting the high-temperature and high-pressure requirements of the test. Accordingly, a bending tool system (Figure 5) was designed, comprising four vertical columns, fixed guides, lateral support/pressure blocks, pneumatic cylinders, as well as a ground plate (max dimensions: 400 × 240 × 300 mm). The support blocks featured 5 mm radii, assuming negligible bending/unloading effects and the pressure blocks were bolted to the upper profile via pneumatic cylinders, allowing adjustable vertical movement.

Experimental procedure

The clamped-beam bending tests were conducted on a Zwick-250 kN machine with a temperature chamber. The bending tool system with two pneumatic cylinders for the concept is installed and fixed on the lower table of the machine, while the bending punch is connected to the upper tool along the vertical centreline for the specimen as presented in Figure 6(a). The load-displacement curve for a given parameter combination can be obtained through the measuring system of the machine. Moreover, the processing temperature is preset by the temperature chamber system while the real-time temperature inside the chamber is recorded by the thermocouples. Other test parameters like punch speed of 10 mm/min and punch displacement of 40 mm are set as constants by the manual input in the machine system. To measure and control the pressure, a real-time pressure tank and manual pressure controller are used as shown in Figure 6(b) and (c). The maximum pressure from the tank is 9 bar, and the air pressure inlets as well as return flow outlets are converged in two separate channels and connected to the tank, respectively. Through the preset value on the controller, the pressure block is able to adjust the load, which alter the stretching length of the specimen along the longitudinal direction.

The material configurations and test conditions used for the clamped-beam bending test of the uncured metal-CFRP laminates are summarized in Table 2. The tests are performed with Al/CFRP and Ss/CFRP laminates, as well as four combinations of layup and fibre orientation, four processing temperatures and four clamping pressures. In addition, the tests are conducted varying one parameter at a time while keeping the other parameters at the baseline value, and at least three specimens are applied for each configuration. The baseline value for bending are the layup and orientation of 2/1 and 0°/90° [Metal/0/90/Metal], processing at room temperature (23°C) as well as clamping pressure of 0 bar. The single-layer metal sheets are characterised using the same specimen geometry under the same conditions compared to the corresponding hybrid laminates. These selected test conditions are based on the industrial applications for the laminate press forming and are used to study the effect on the flexural behaviour, in particular the bending force evolution during the clamped-beam bending process.

Finite element model

The application of a finite element model made it efficient to analyse the proposed clamped-beam bending process and support the results from the actual experimental tests. In the

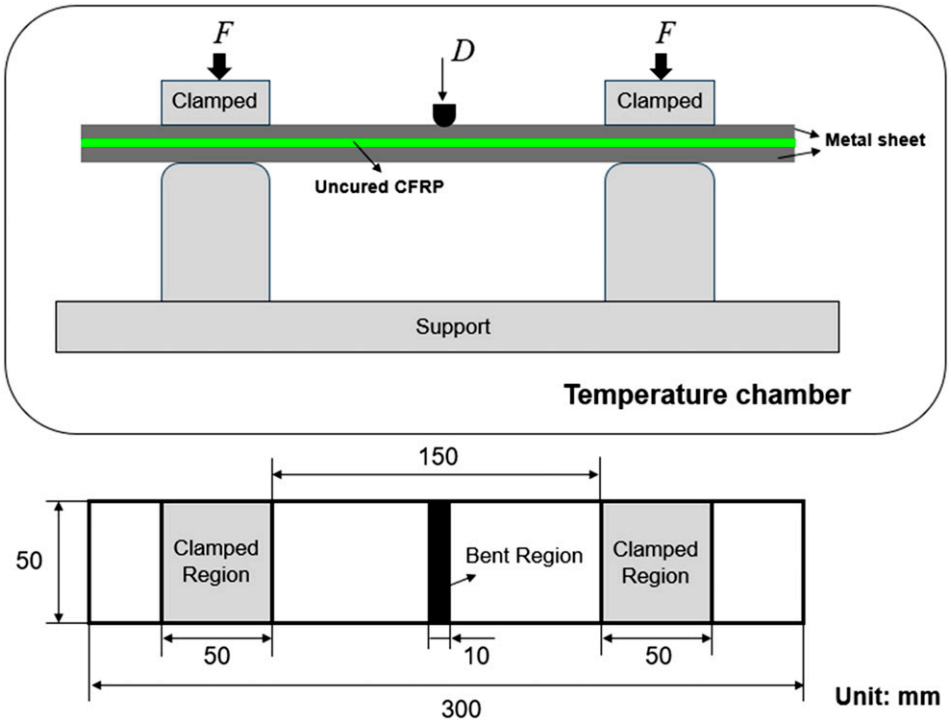

Figure 3. Schematic graph and specimen dimensions for the laminate clamped-beam bending concept.

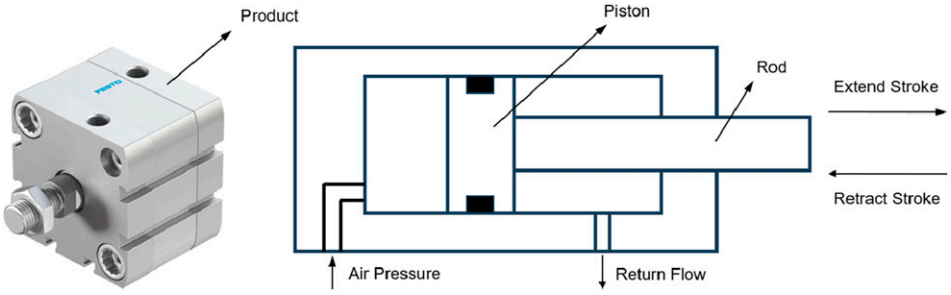

Figure 4. Double-acting pneumatic cylinder and the schematic graph of the pressure loading concept.

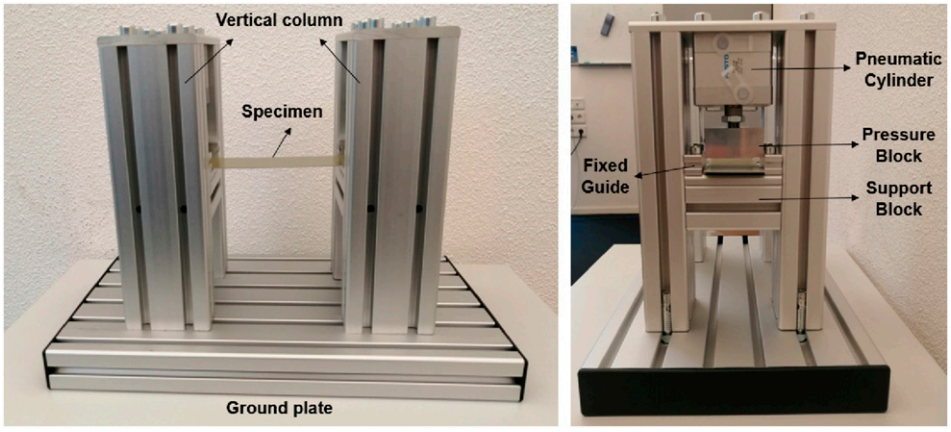

Figure 5. Bending tool system with two pneumatic cylinders for the clamped-beam bending concept.

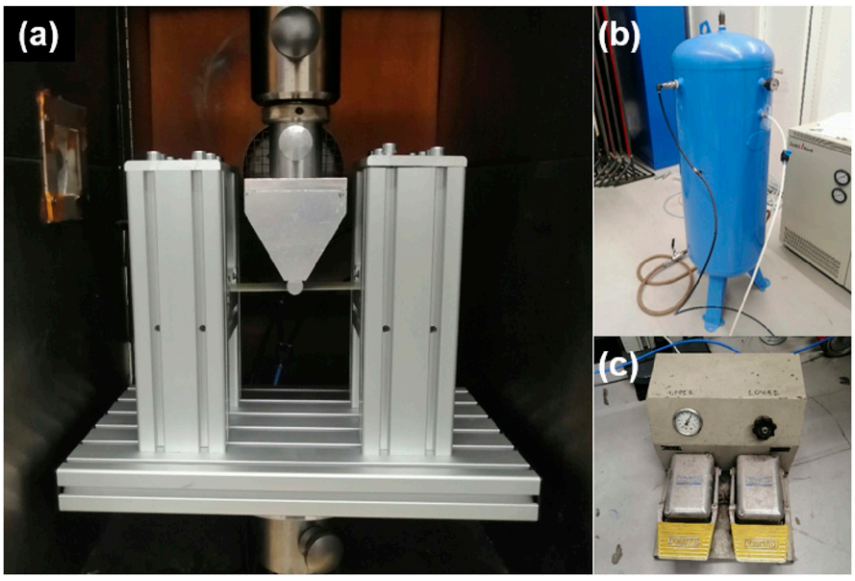

Figure 6. Experimental procedure and apparatus of the laminate bending: (a) Clamped-beam bending setup; (b) Real-time pressure gauge tank; (c) Manual pressure controller.

Table 2. Material configurations and test parameters used for the clamped-beam bending test.

Parameter	Material configuration			
Metal sheet	Aluminium 2024-T3		Stainless-steel 304L	
Fibre prepreg (UD)	CFRP (T300-MTC510)			
Layup and orientation	2/1 (0°/90°)	2/1 (45°/−45°)	3/2 (0°/90°)	3/2 (45°/−45°)
Processing temperature (°C)	23 (RT)	50	80	110
Clamping pressure (bar)	0	1	3	6

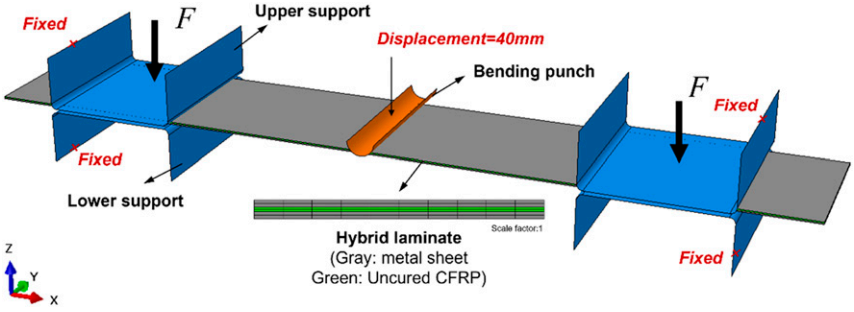

Figure 7. Finite element model of the clamped-beam bending test for the uncured metal-CFRP laminates.

study, finite element analysis software Abaqus is used to simulate the bending procedure of the uncured metal-CFRP laminates by using the stress-strain distributions of the metal sheet and the unique anisotropic properties of the carbon fibre reinforced prepreg (CFRP). Figure 7 exhibits the simulation model established for the research and all the materials as well as tool geometries followed the concept of the experimental setups. The elastic-plastic properties of the metal sheets and the elastic constants for the uncured CFRP lamina as shown in Figure 8 and Table 1 are imported into the material property module in the Abaqus software. In the finite element model, all tools including the bending punch, upper and lower supports are modelled as discrete rigid shell elements with a mesh size of 2 mm. Metal sheets and the uncured CFRP material are all created as four-node doubly curved conventional shell elements with reduced integration (S4R) in a same mesh size of 2 mm. The laminate structure in the FE model is represented in the composite layup

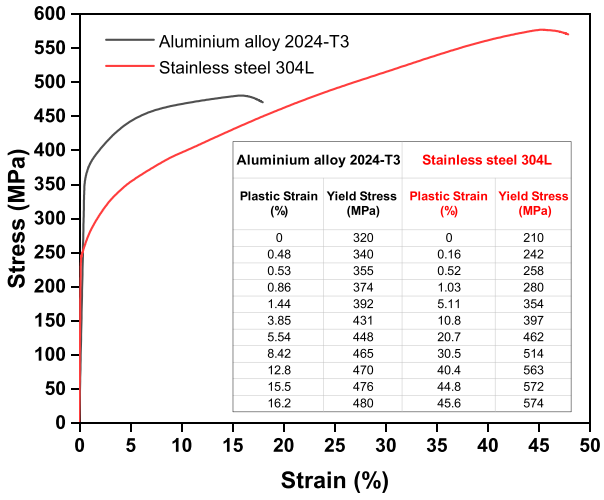

Aluminium alloy 2024-T3		Stainless steel 304L	
Plastic Strain (%)	Yield Stress (MPa)	Plastic Strain (%)	Yield Stress (MPa)
0	320	0	210
0.48	340	0.16	242
0.53	355	0.52	258
0.86	374	1.03	280
1.44	392	5.11	354
3.85	431	10.8	397
5.54	448	20.7	462
8.42	465	30.5	514
12.8	470	40.4	563
15.5	476	44.8	572
16.2	480	45.6	574

Figure 8. Stress-strain curve of the metal sheets applied for the clamped-beam bending test simulations.

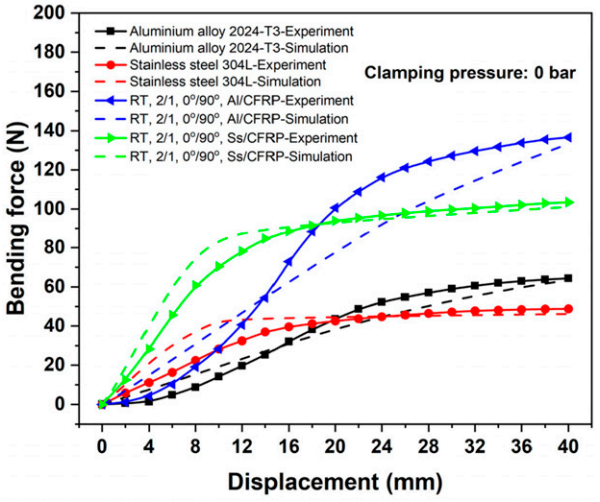

Figure 9. Experimental and numerical results on the bending force evolution of the metal sheet and the corresponding metal-CFRP laminate at room temperature (RT) with the clamping pressure of 0 bar.

module where all layers and their parameters such as orientation, thickness, property and relative location are defined and assembled into the bending simulation. As for the interactions and boundary conditions in the model, the value of clamping force and displacement (40 mm) can be set, and the contacts between the fixed upper and lower supports, as well as uncured metal-CFRP laminates are set as penalty friction in a constant value of 0.15. The interaction at the metal-prepreg interfaces is defined as friction contact which consists of the mechanical elastic and viscous flow. A static-kinetic exponential decay model in Abaqus is applied to simulate the transition of friction and the value can be obtained from a previous study.[13] In order to characterise and validate the flexural behaviour of the test materials, the load-displacement response in the Static/Standard step, and the spring-back depth as well as the length reduction coupled with plastic deformation in the Dynamic/Explicit step are analysed and compared with the experimental results.[34,38]

Results and discussion

Bending load-displacement response

Effect of metal composition. During the clamped-beam bending process, he load-displacement response serves as one of the most quantitative indicators for characterizing the flexural behaviour of test materials. Figure 9 presents both experimental and simulation results of the bending load-displacement response under unclamped conditions at room temperature. During the initial bending stage, the simulated bending force increases slightly faster than observed in experimental conditions. This discrepancy primarily results from the delayed response of the testing machine during initial punch-specimen contact. However, as punch displacement progresses, the bending forces gradually converge, reaching agreement at 40 mm displacement. The consistency in maximum bending force value validates both the test methodology and finite element model by the bending process conclusion. Regarding the metal composition effects, the maximum bending force for single-layer aluminium alloy 2024-T3 and Al/CFRP laminate exceeds that of single-layer stainless-steel 304L and corresponding Ss/CFRP laminate under identical configurations. Additionally, stainless-steel-based materials exhibit earlier force stabilization during bending. This behaviour correlates with the stress-strain curves shown in Figure 8, which indicates that the aluminium alloy has a higher yield stress than the stainless-steel, generating greater punch reaction forces. Conversely, the lower yield stress of the stainless-steel causes earlier plastic deformation initiation, resulting in slower subsequent stress and bending force development.

Moreover, it can be obtained from Figure 9 that the maximum bending force of the uncured metal-CFRP laminate is higher than the sum force of two single-layer metal sheets under the same test conditions. One reason is that the uncured hybrid laminates are deformed independently from each other, the required bending moments are sum of bending all these sheets. Other explanations can be obtained from the differences of the stress distribution through the thickness direction after bending as shown in Figure 10. The bending deformation of the metal sheet is simplified as a material exhibiting elastic-ideal plastic behaviour without hardening. For a single-layer metal sheet, the stress distribution is symmetrical along the neutral layer where the metal surfaces 1&2 undergo the maximum tensile stress and compressive stress, respectively. In the outer

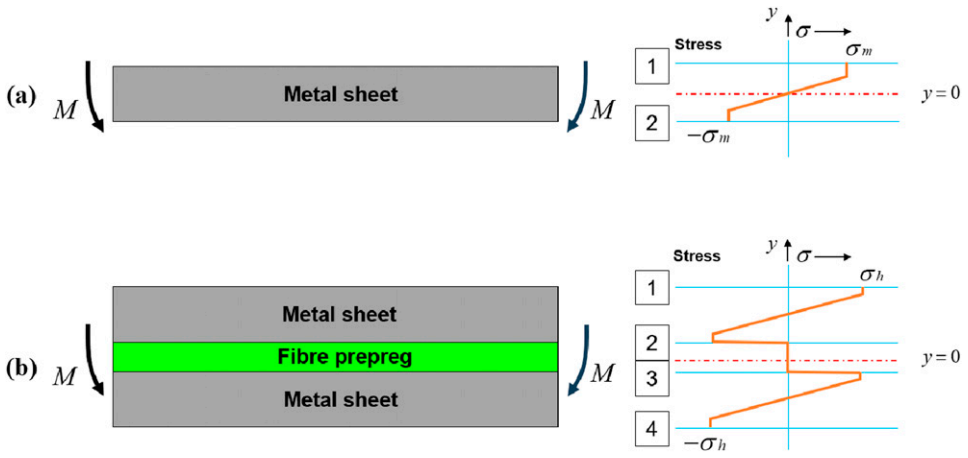

Figure 10. Schematic graph of the stress distribution after bending process for different test materials: (a) Single-layer metal sheet; (b) uncured metal-composite laminate with 2/1 layups.

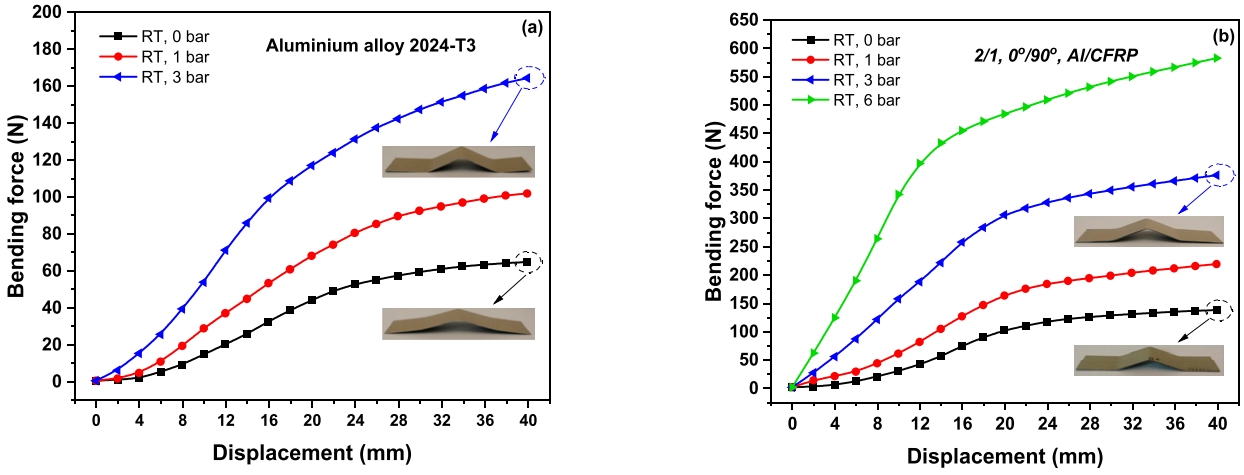

Figure 11. Experimental bending force and displacement curves under various clamping pressures for clamped-beam bending test: (a) Single-layer aluminium alloy 2024-T3; (b) 2/1, 0°/90° Al/CFRP at room temperature of 23°C.

surfaces, the stress will be capped at the maximum stress σ_m where the vertical lines denote the plastic deformation areas. The outer surfaces 1&4 for a hybrid laminate with the 2/1 layup experience the same stress state as the metal sheet, while the metal sheets and fibre prepreg deform independently from each other when the hybrid laminate is bent with an uncured fibre prepreg in the middle. The inner surfaces (2&3) of the metal sheet could slip over the prepreg layer and the sliding resistance depends on the friction at the metal-prepreg interfaces. Besides, it is noted that the maximum bending force for Al/CFRP and Ss/CFRP laminate with a 2/1 layup is slightly over twice the value than their corresponding single-layer metal sheet. The finding shows that the bending properties of the hybrid laminates depend mainly on the properties of metal sheets while the uncured CFRP material plays a limited role.

Effect of clamping pressure. The application of clamping pressure is one of the focus points in the research and the investigation of clamping effects on the flexural behaviour of uncured laminates becomes significant. Figure 11(a) and (b) exhibit the experimental bending force and displacement curve of the single-layer aluminium sheet and the Al/CFRP laminate under different clamping pressures, respectively. The uncured Al/CFRP laminates are tested at room temperature (23°C) with a layup of 2/1 and fibre orientation of 0°/90°. For the bending of the single-layer aluminium alloy shown in Figure 11(a), the bending force gradually increases with the punch movement and the increase of clamping pressure from 0 bar to 3 bar increases the bending force with displacement of the punch. When replacing the single-layer metal sheet with an Al/CFRP laminate with a specific configuration, the bending force increases until it reaches the maximum value at the end of the bending test as

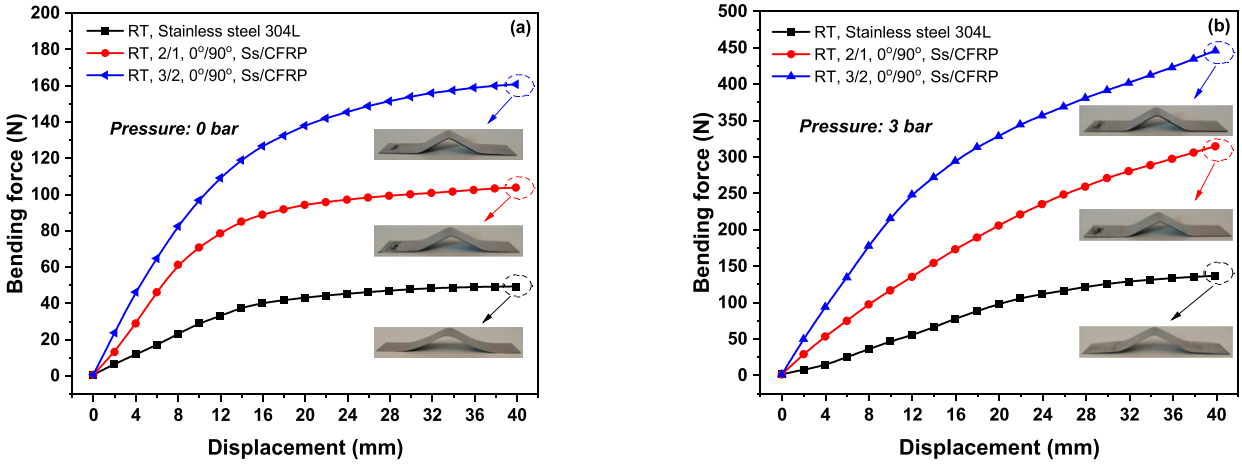

Figure 12. Experimental bending force and displacement curves of the single-layer stainless-steel and its corresponding hybrid laminates at room temperature (23°C) for clamped-beam bending with two clamping pressures: (a) 0 bar; (b) 3 bar.

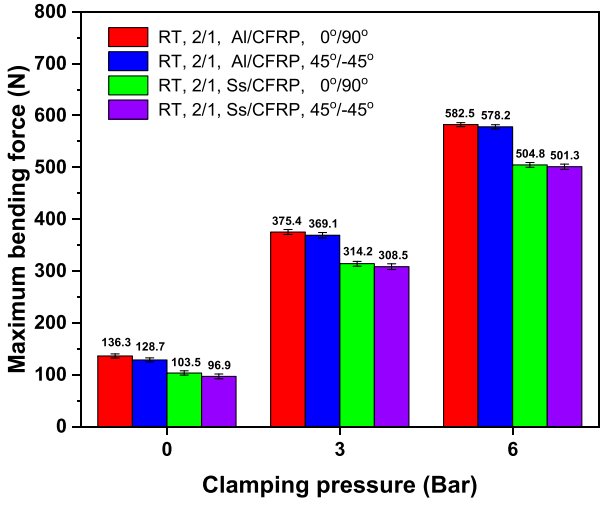

Figure 13. Experimental results for the maximum bending force of different laminate structures under three clamping pressures.

well. The result validates that clamping pressure plays a significant role in the bending force of both metal sheet and the hybrid laminates. However, although all the test materials experience growth in bending force with the increase of punch displacement, the trends of increase are different when applying different clamping pressures. When there is no clamping pressure on the clamped regions, the bending force grows significantly at the initial stage of bending and gradually goes towards a nearly constant value until the end of the bending test. As the pressure increases, the increase in bending force becomes more distinct and the stage where the force tends to level off earlier in the bending process. One of the explanations is that the increase of clamping pressure restricts the material flow in longitudinal direction, which requires greater bending force to achieve the same amount of deformation. It can also be explained through the increase of plastic strain at the same displacement with the increase of clamping pressure. As shown in Figure 8 that a higher force (stress) induces more plastic strain and an earlier start of plastic deformation. It can be observed from the bent specimens of the aluminium alloy 2024-T3 in Figure 11(a) that the single-layer aluminium sheet under the clamping pressure of 3 bar undergoes larger plastic deformation and becomes more pronounced compared to the bent aluminium sheet without clamping pressure. The effect of clamping pressure on the bending force for the hybrid laminate is even greater since the force scale runs from 0 to 600 N as shown in Figure 11(b). The reason is due to the increase of bent layers and frictional force at the tool-metal and metal-prepreg interfaces which hinder the sliding, making the stress σ_m and σ_h greater than the bent material without clamping pressure. More details on the effect of clamping pressure on material plastic deformation will be discussed.

Effect of layup and fibre orientation. In order to investigate the effect of laminate layup on the bending force, the Ss/CFRP laminates of 2/1 and 3/2 layups at room temperature (23°C) with the fibre orientation of 0°/90°, as well as the single-layer stainless-steel are compared. Experimental results on the bending force evolution of the three materials under the clamping pressures of 0 bar and 3 bar are shown in Figure 12. It is obvious that the increase of laminate layup from a single-layer metal sheet to a 3/2 hybrid laminate contributes to the increase of bending force. The increasing number of layers dominates the growth of bending force which follows the conclusions of the three-point bending and the fixed-beam bending studies from literature.[39,40] Besides, it is obtained from the results that the bending force is determined by the metal sheets whereas the composite layers hardly contribute since the uncured laminates

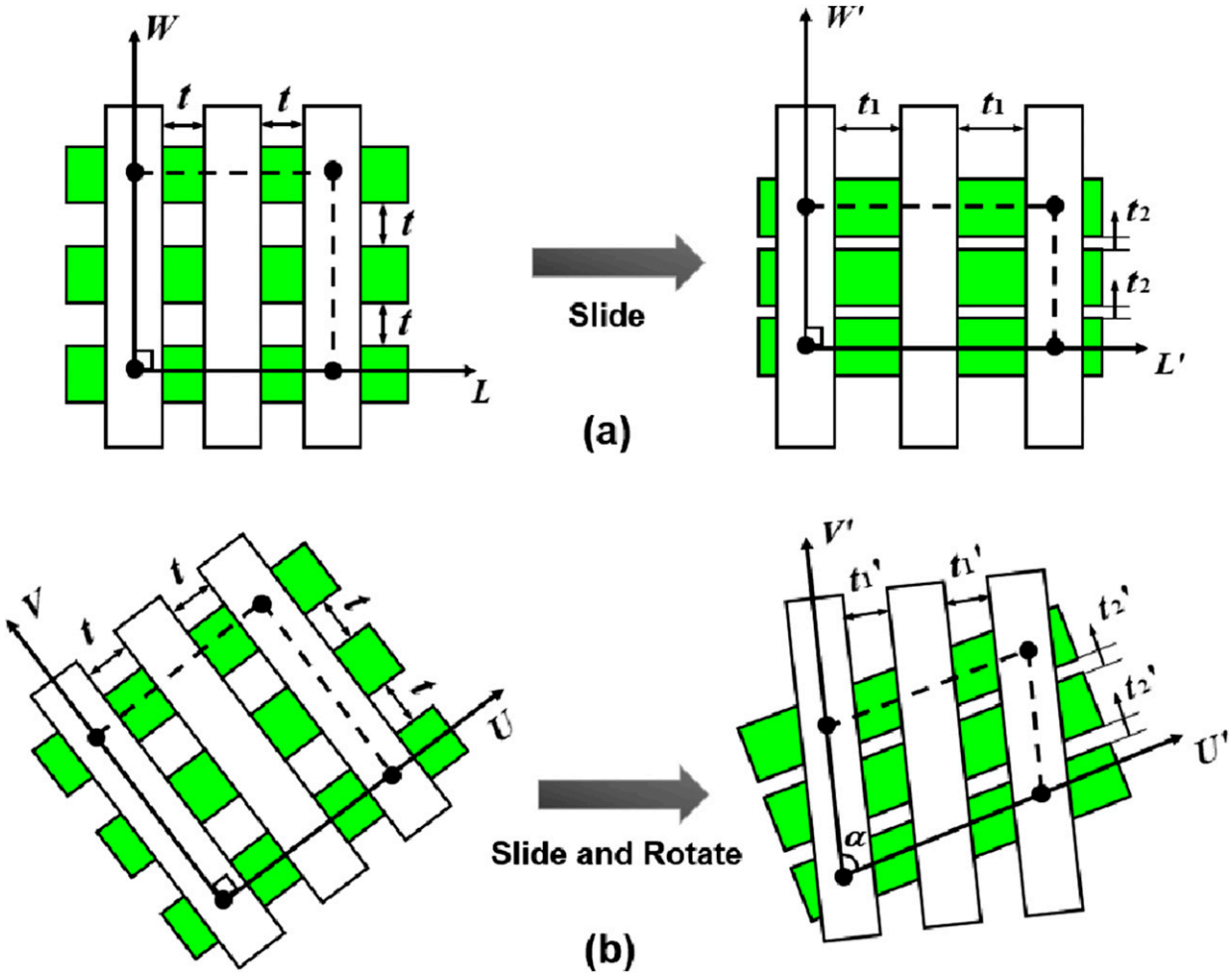

Figure 14. Schematic graph of the deformation mechanisms during bending for two typical fibre orientations of cross-ply UD prepregs: (a) 0°/90°; (b) 45°/−45°.

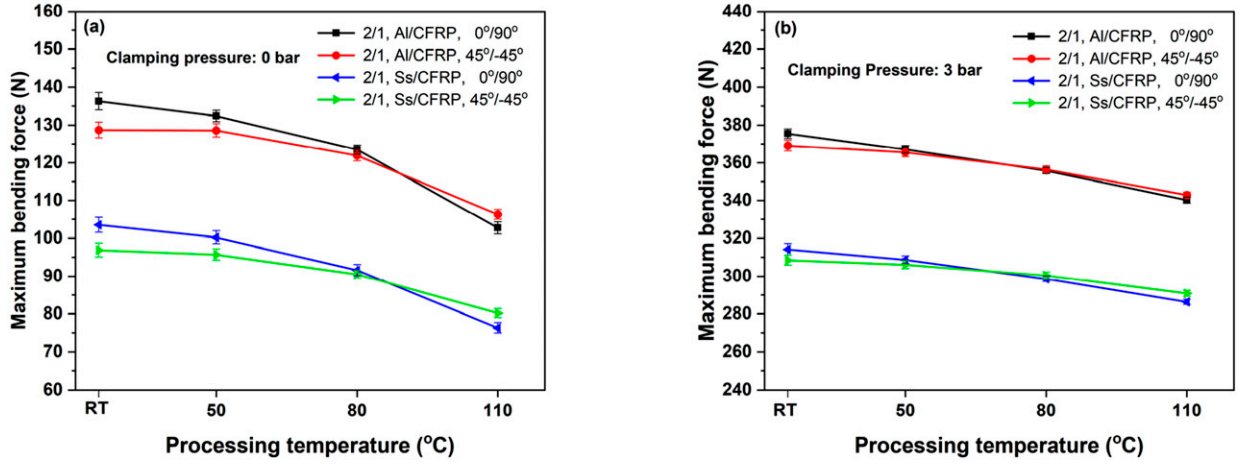

Figure 15. Experimental results on the maximum bending force under different processing temperature and pressure conditions for the hybrid laminate of 2/1 layups: (a) 0 bar; (b) 3 bar.

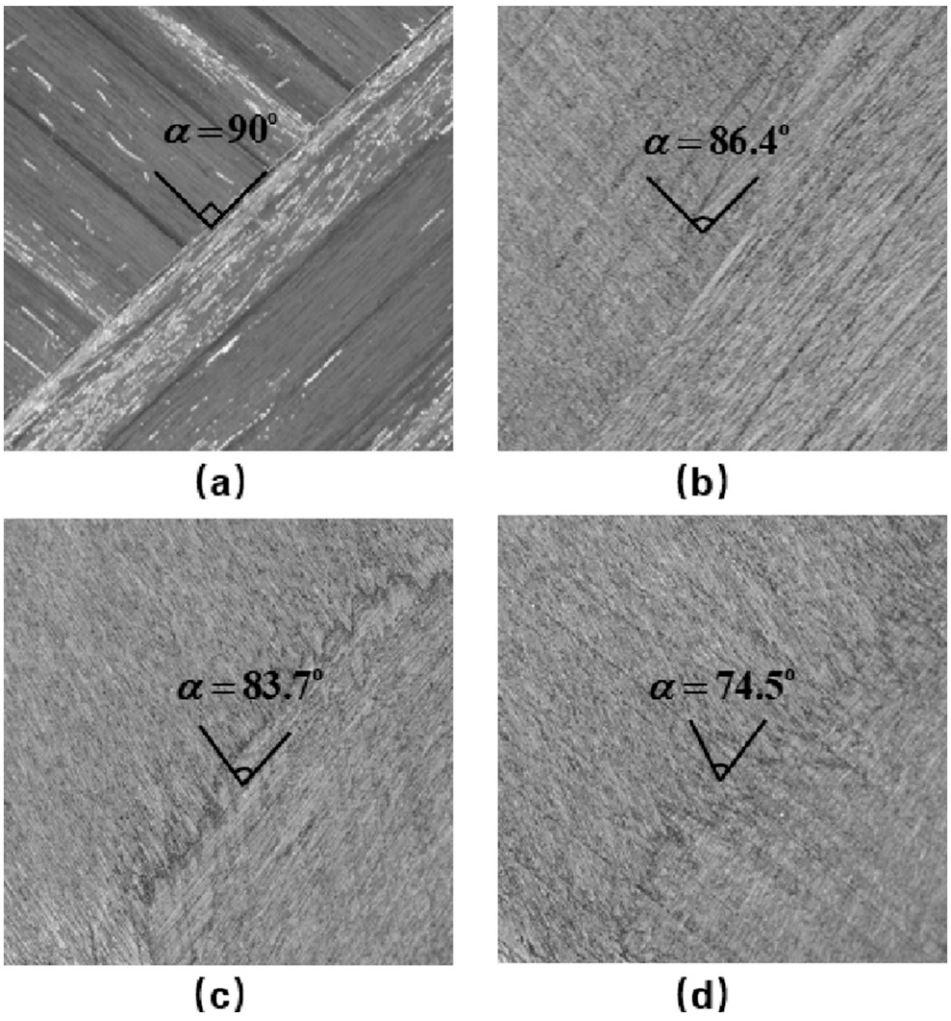

Figure 16. Microscopic measurements of the rotation angle α on the centre region of the 2/1, Al/CFRP laminate with the fibre orientation of 45°/−45° under various bending conditions: (a) Initial state; (b) RT, 0 bar; (c) 80°C, 0 bar; (d) 80°C, 3 bar.

act independently. The bent specimens of the Ss/CFRP laminates under two clamping pressure conditions are more pronounced and has an increased remaining bent depth after unloading when compared to the single-layer stainless-steel. More details on the spring-back effect will be discussed in section "Spring-back depth". For the effect of fibre orientation, the cross-ply unidirectional CFRP materials of 0°/90° and 45°/−45° for the metal-CFRP laminates of a 2/1 layup are compared. Figure 13 exhibits the test results of the maximum bending force for four different laminate structures under three clamping pressures at room temperature (23°C). It can be observed from the figure that the hybrid materials with a fibre orientation of 45°/−45° have slightly smaller bending force due to the intra-ply shear at the maximum displacement than the metal-CFRP laminates with the fibre orientation of 0°/90° under the same conditions.

Figure 14 describes two deformation mechanisms during the bending process for the CFRP materials in the hybrid laminates. Bending of cross-ply unidirectional (UD) structure with a fibre orientation of 0°/90° mainly involves slide at the prepreg-prepreg interface. Assuming that the gaps between each fibre tow at the initial state are a constant value t, and the gaps after bending along a new axis of L' and W' between the fibre tow are t_1 and t_2, respectively. It is noted that the $L-W$ and $L'-W'$ coordinate system are kept as vertical during bending and the relationship between the tow-gap is $t_2 < t < t_1$. However, the kinematics of the cross-ply unidirectional (UD) structure with a fibre orientation of 45°/−45° are different where the adjacent plies of the fibre prepreg rotate and slide over each other and are coupled through a viscous resin. The vertical coordinate system $U-V$ gradually changes into a new coordinate system $U'-V'$ with a rotation angle α. Although the gaps

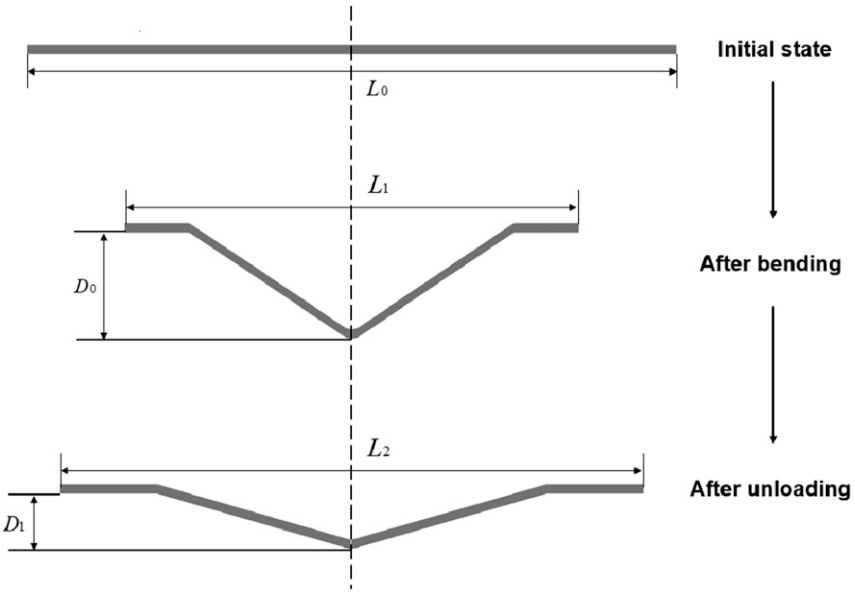

Figure 17. Schematic graph and dimension of three different stages during the laminate bending process.

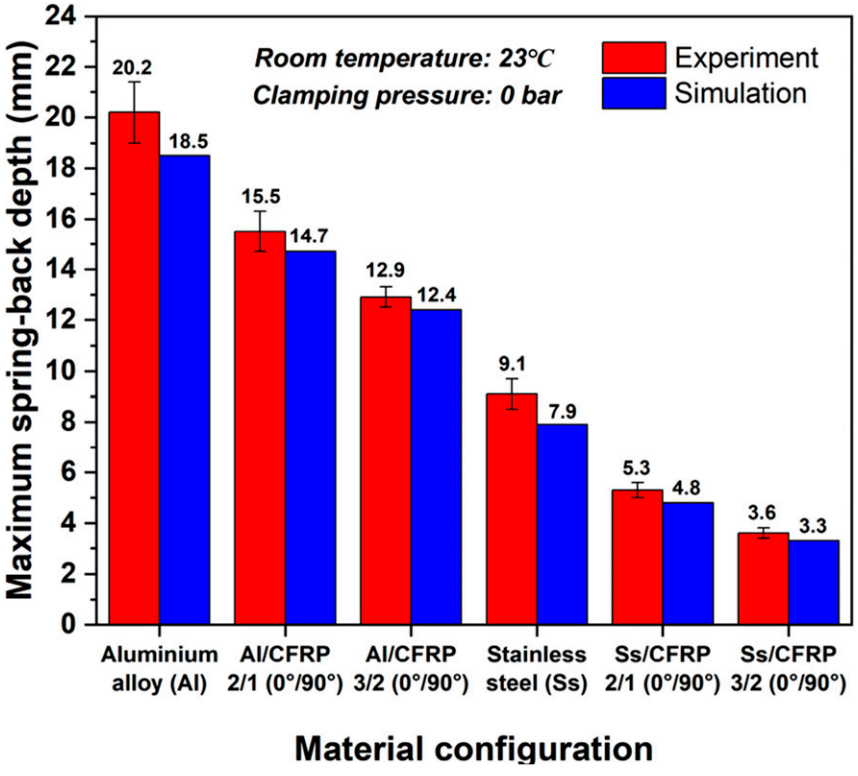

Figure 18. Experimental and numerical comparisons on the spring-back depth for different material configurations.

of fibre tow after bending still follow the relationship of $t_2' < t < t_1'$, the relationship between the gaps of fibre tow for the 45°/−45° and 0°/90° structures is $t_1 > t_1' > t, t > t_2' > t_2$ due to the existence of prepreg rotations at the same deformation. Therefore, the different deformation mechanisms for the hybrid materials with a fibre orientation of 45°/−45° and 0°/90° affect the maximum bending force during bending.

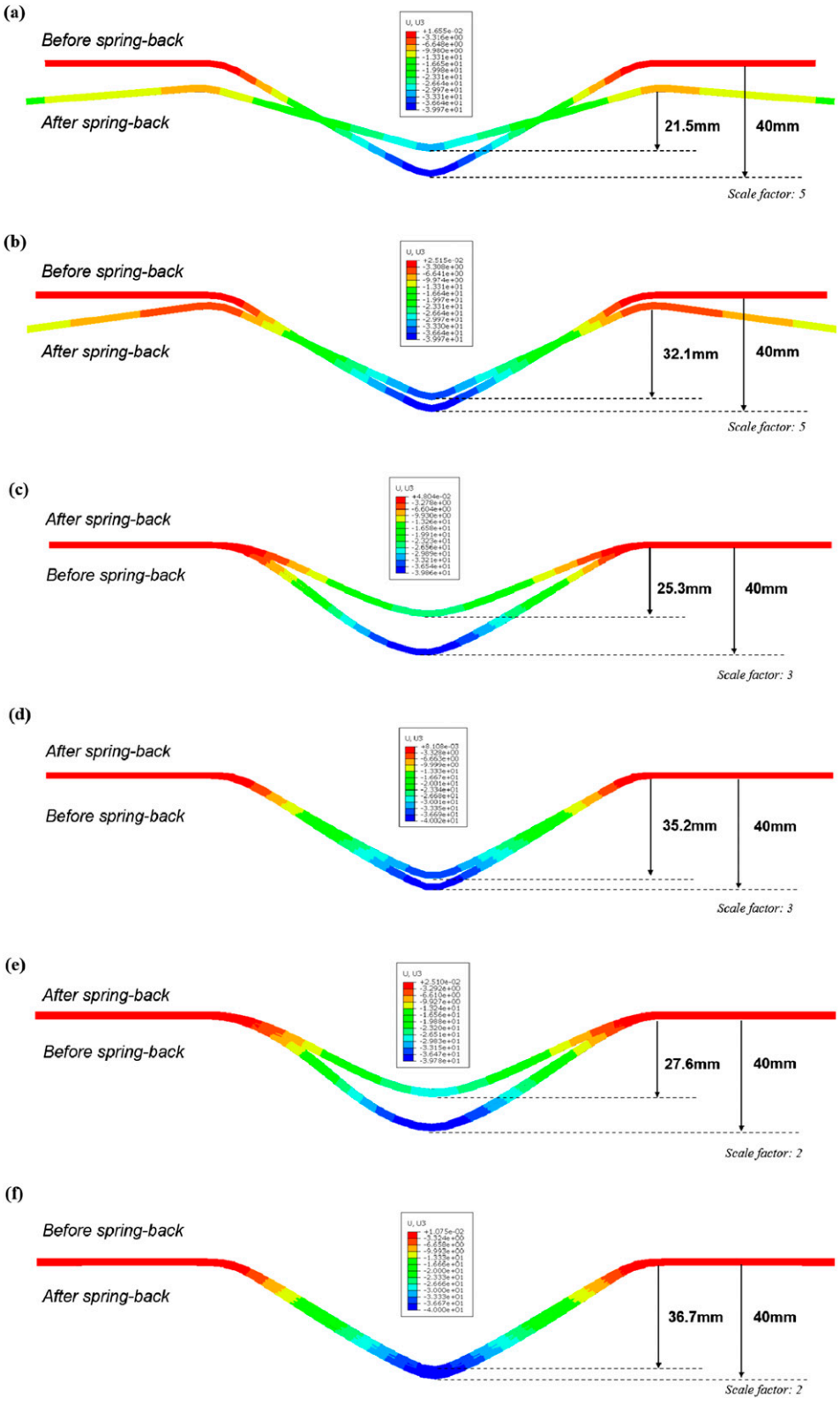

Figure 19. Numerical results of the vertical displacement (U_3) before and after spring-back of bending for different materials under the conditions of no clamping pressure and room temperature (23°C): (a) Single-layer aluminium alloy 2024-T3; (b) Single-layer stainless-steel 304L; (c) 2/1, 0°/90°, Al/CFRP; (d) 2/1, 0°/90°, Ss/CFRP; (e) 3/2, 0°/90°, Al/CFRP; (f) 3/2, 0°/90°, Ss/CFRP.

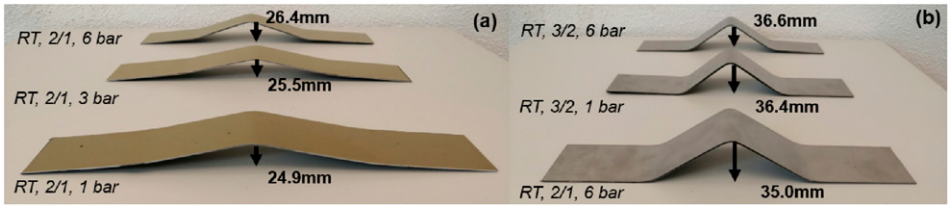

Figure 20. Test specimens after spring-back for different laminate configurations and test conditions at room temperature: (a) 2/1, 0°/90°, Al/CFRP laminates; (b) 0°/90°, Ss/CFRP laminates.

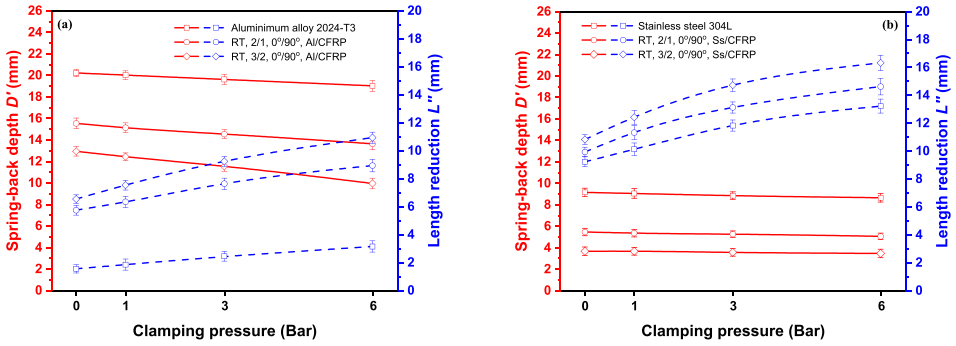

Figure 21. Experimental results on the spring-back depth and length reduction after unloading under various pressure conditions: (a) Aluminium alloy based materials; (b) Stainless-steel based materials.

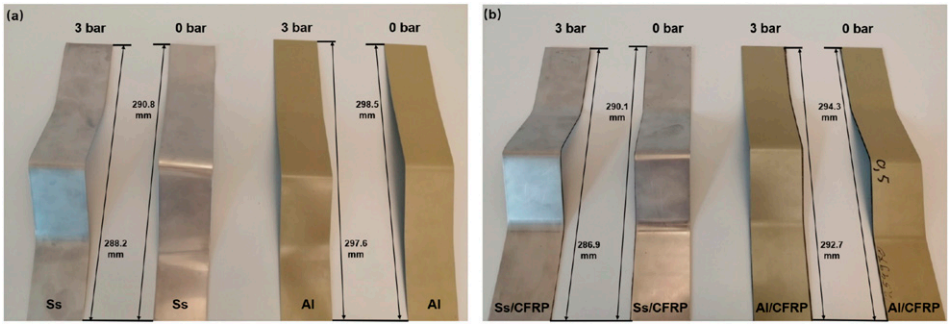

Figure 22. Test specimens under two clamping pressure conditions at room temperature for different materials after spring-back: (a) Single-layer metal sheets; (b) 2/1, 0°/90°, hybrid metal-CFRP laminates.

Effect of processing temperature. The processing temperature is also a crucial factor affecting the bending force since the elastic modulus of the uncured CFRP materials, as well as the frictional force at the metal-prepreg interfaces and prepreg-prepreg interfaces are temperature-dependent. Figure 15 exhibits the experimental results of the maximum bending forces at four different processing temperatures under the clamping pressure of 0 bar and 3 bar. The two curves reveal that the maximum bending force decreases with increase of temperature, while the magnitude of decrease is different for the uncured 2/1 hybrid laminates with a fibre orientation of 45°/−45° and 0°/90°. When the pressure applied on the clamped regions is zero, the maximum bending force for Al/CFRP and Ss/CFRP laminates with the 45°/−45° structure at the processing temperature of 110°C is higher than their corresponding laminates with the 0°/90° structure. At room temperature, the result is the other way around. There are two reasons which helps to explain the bending force reduction. Firstly, due to the resin viscosity decrease with the temperature increases, the softening of CFRP material decreases the overall elastic modulus and thus, lower the bending force. Then, the frictional force at the interfaces of each layer decreases significantly as the temperature increases, which further reduces the maximum bending force for the uncured laminates. This can be referred to Figure 10(b) where the

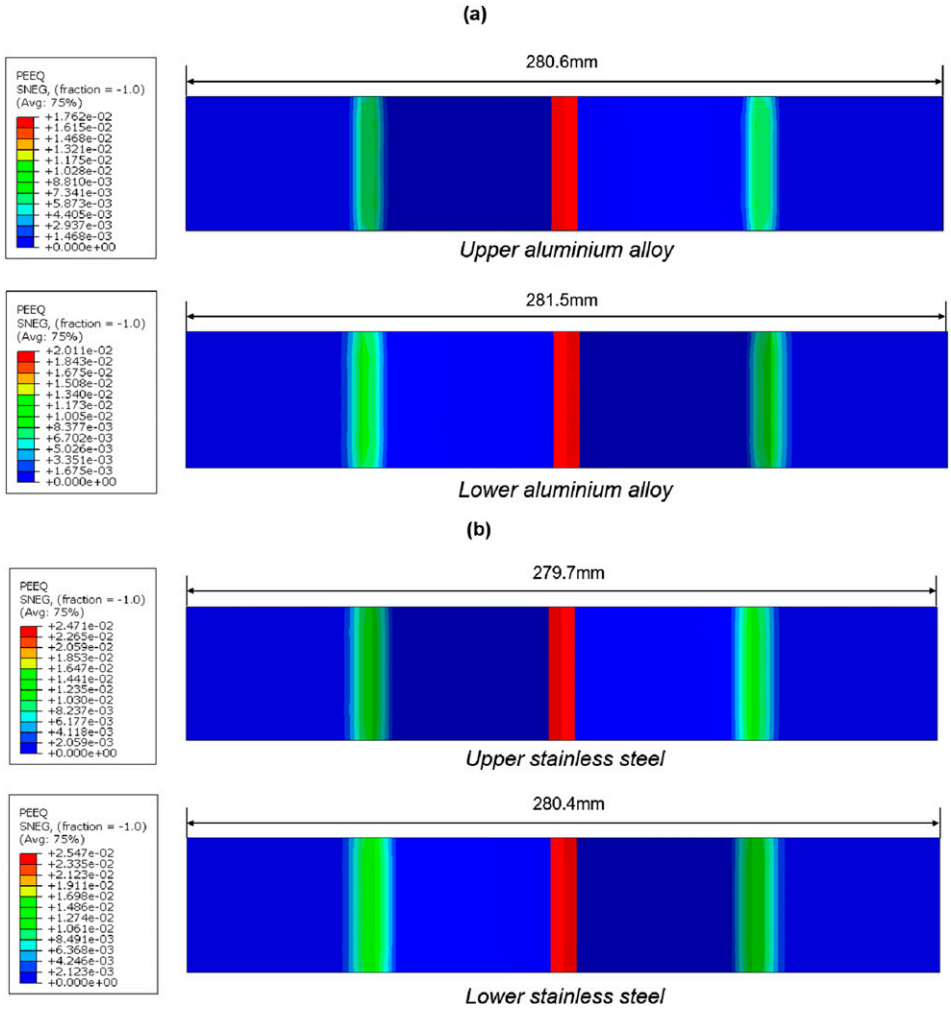

Figure 23. Numerical results on the equivalent plastic strain at room temperature for hybrid laminates after bending. (a) RT, 2/1 Al/CFRP laminate, Clamping pressure: 0 Bar, (b) RT, 2/1 Ss/CFRP laminate, Clamping pressure: 0 Bar, (c) RT, 2/1 Al/CFRP laminate, Clamping pressure: 6 Bar, (d) RT, 2/1 Ss/CFRP laminate, Clamping pressure: 6 Bar.

stress σ_h for laminate bending decreases since the sliding at the metal-prepreg interfaces is easier. However, the hybrid structures with 45-degree layers at least offers more contributions on the bending moment than the 90-degree layers, which seem contrary to the trend of force reduction.

The previous study[14] also found that the temperature effect dominates the in-plane shear force for the cross-ply UD fibre reinforced metal laminates with 45°/−45° structures. Once the increased bending moment and shear force accumulate to a certain value, the 45°/−45° structures need a greater maximum bending force at a certain temperature for the 45°/−45° structures than the 0°/90° structures which only experience the inter-ply sliding during bending. Besides, the increase of clamping pressure hinders the sliding of the uncured metal-CFRP laminates, which further increases the shear force at the same displacement for 45°/−45° structures. This reveals that the maximum bending force becomes larger for low temperature and high pressure conditions. The microscopic measurement for the rotation angle α on the central regions of the 2/1 Al/CFRP laminates with the fibre orientation of 45°/−45° are applied[12] and the results under various bending conditions are shown in Figure 16. The results for the angle measurement prove that the increase of clamping pressure and temperature helps to decrease the rotation angle α.

Laminate bendability characterisation

Spring-back depth. The evolution of spring-back after the clamped-beam bending process can also be used for the characterisation of the flexural behaviour of the test materials. The experimental and numerical simulation methods are applied to study the differences of the bent materials before and after spring-back as exhibited in Figure 17. The values of spring-back depth for various material configurations at room temperature without clamping pressure are

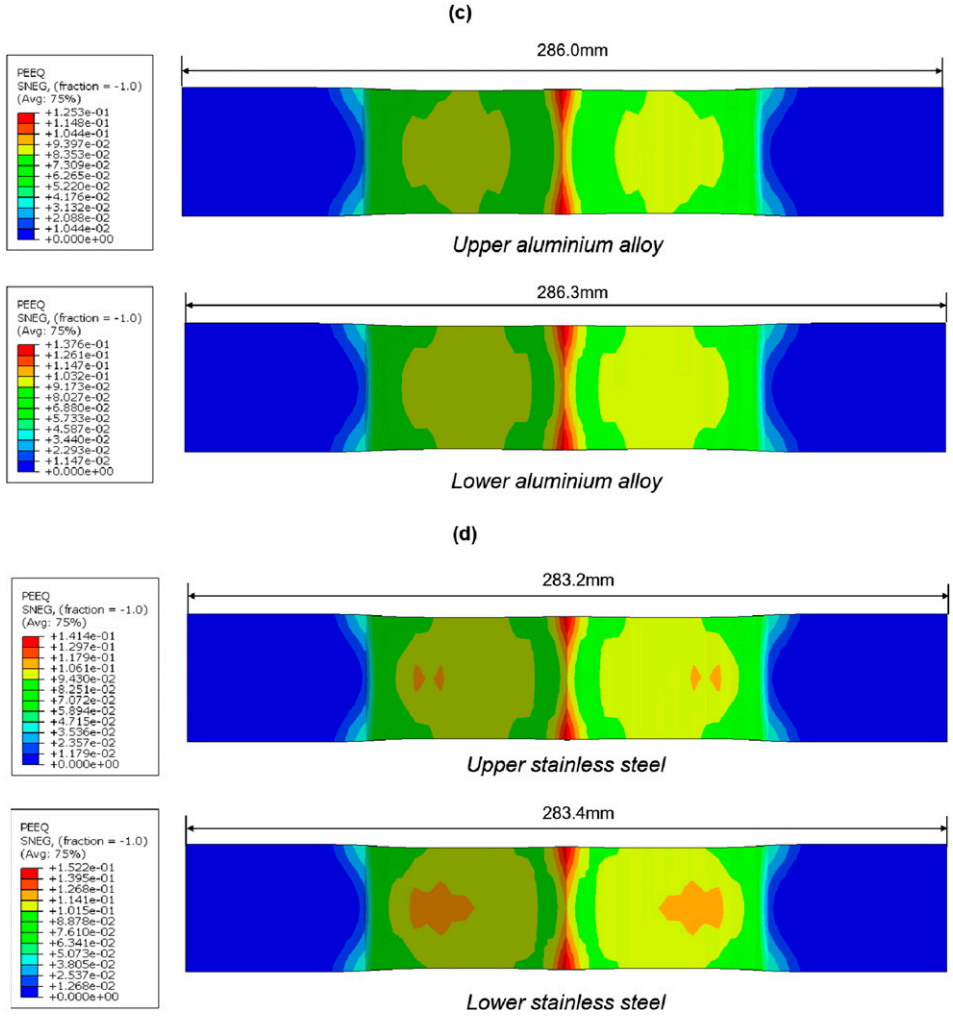

Figure 23. Continued.

shown in Figure 18. The spring-back depth D' is measured by the differences of the bending depth before and after spring-back ($D' = D_0 - D_1$). The effect of fibre orientation and processing temperature on the spring-back depth for the uncured metal-CFRP laminates are not investigated as the effects can be ignored. The test and simulation results reveal that the aluminium based materials experience more spring-back than stainless-steel based materials and the increase of laminate layup would reduce the spring-back depth. This can also be explained from the stress-strain curve presented in Figure 8, where the higher elastic modulus and lower yield strength of the stainless-steel result in a lower elastic response compared with the aluminium alloy when the metal sheet reaches the same amount of deformation. Furthermore, the increase of laminate layup also plays a significant role in the spring-back reduction where the bending radius of the outer sheet of the uncured laminates is larger than the single-layer sheet, which have a huge impact on the strain distribution of that layer and its elastic response.[41,42] Therefore, the spring-back depth of the metal-CFRP laminates are lower than their corresponding single-layer metal sheets. The numerical colourmaps of the vertical displacement (U_3) before and after spring-back for various material configurations at room temperature without clamping pressure are shown in Figure 19. It is observed that the vertical displacement and shapes after unloading for the single-layer metal sheets and hybrid laminates are different. As the thickness of a single-layer metal sheet is small, the bent materials at centre and flange regions undergo opposite displacement after unloading without clamping pressure on the flange regions. However, the increase of layup and bending radius gradually hinders the vertical movement and the materials become flat on the flange regions.

The experimental tests on the depth of laminate spring-back are also performed under different clamping pressure

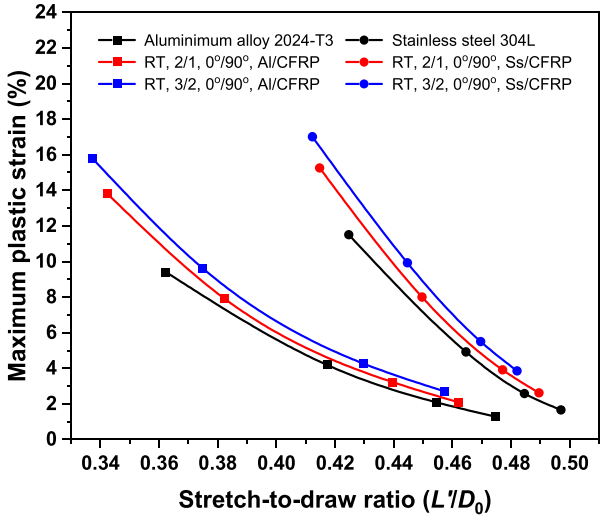

Figure 24. Numerical results on the relationship of maximum plastic strain and stretch-to-draw ratio for different materials.

conditions. Figure 20 shows the test specimens after spring-back for different laminate configurations and test conditions at room temperature, and the spring-back depth D' for the aluminium-based and stainless-steel-based materials under various pressure conditions are shown in Figure 21(a) and (b). All the curves on the evolution of spring-back depth show that the increase of clamping pressure contributes to the reduction of spring-back. The results are also visible in Figure 20 where the introduction of an increasing tension force in the laminates decreases the out-of-plane spring-back. However, it can be seen from the curves that the decreasing trend of spring-back is different for the Al/CFRP and Ss/CFRP laminates with the increase of clamping pressure. The Al/CFRP laminates show more obvious spring-back decrease when the pressure increases especially for the 3/2 layups, while the effect of clamping pressure on the spring-back reduction for the Ss/CFRP laminates is limited. Although the spring-back depth for the Ss/CFRP laminate itself is small, the influence of laminate layup dominates the spring-back process when the bending punch is unloaded.

Length reduction. Due to the application of clamping pressure on the local flange regions of the specimen, the length reduction along the longitudinal direction is also an index for the characterisation of the flexural behaviour. Therefore, the study of the clamping pressure effect on the length variations before and after unloading is proposed, and the factors affecting the properties of CFRP material such as fibre orientation, processing temperature are not studied as the variations on the bent length is quite small. The length reduction after unloading L'' is defined and calculated by the differences of the initial longitudinal length and the bent length after unloading ($L'' = L_0 - L_2$) which described in Figure 17. The initial longitudinal length is 300 mm and the bent lengths after unloading for the test materials under two clamping pressure conditions at room temperature are shown in Figure 22. It is seen that all the materials undergo the length reduction after bending and unloading under the pressure conditions. The increasing clamping pressure decreases the bent length L_2 to some extent as more plastic deformation remains on the bent materials after unloading. In addition, the curves on the length reduction L'' under various pressure conditions as shown in Figure 21(a) and (b) reveal that the aluminium-based materials have smaller length reduction compared to the stainless-steel-based materials especially for the single-layer metal sheet. The reason is mainly because of the higher elastic response after unloading for the aluminium sheet where the bent length is closer to the initial length. Besides, the result shows that the increase of laminate layup leads to an increase on the length reduction for the bent laminates and the sliding resistance become more significant under higher clamping pressure conditions.

Plastic deformation. To quantify the effect of clamping pressure on the flexural behaviour of uncured metal-CFRP laminates, the relationship between plastic deformation evolution and the stretch-to-draw ratio is investigated. Since the laminate unloading involves only elastic recovery without plastic deformation, the stretch-to-draw ratio is defined as the ratio of length reduction before unloading to the initial bending depth (L'/D_0). The initial bending depth D_0 was set at 40 mm, while the length reduction before unloading L' was calculated as the difference between initial longitudinal length and the bent length prior to unloading. Figure 23 presents numerical colormaps of equivalent plastic strain for hybrid laminates before unloading. The results show that under both pressure conditions, the upper metal surfaces of 2/1 layup metal/CFRP laminates exhibited smaller bent lengths before unloading and lower equivalent plastic strains compared to the lower metal surfaces. This phenomenon can be attributed to interfacial sliding at metal-prepreg interfaces and the stress distribution pattern shown in Figure 10(b). At 0 bar clamping pressure, the maximum equivalent plastic strains for Al/CFRP and Ss/CFRP laminates were approximately 2.01% and 2.55%, respectively, despite their similar strain distributions. However, when the pressure increased to 6 bar, the plastic strain distribution changed significantly: strains increased in unsupported regions of the bent laminates, with maximum equivalent plastic strains occurring along the centreline edges, reaching 13.76% and 15.22%, respectively. Figure 24 illustrates the influence of stretch-to-draw ratio on plastic deformation, based on numerical results of pre-unloading bent lengths and equivalent plastic strains. The data demonstrate that maximum plastic strain decreases with increasing stretch-to-draw ratio for all materials, with this trend becoming

more pronounced as laminate layup increases. Furthermore, stainless-steel-based materials exhibited higher stretch-to-draw ratio and greater plastic deformation than aluminium-based materials under identical conditions. These findings indicate that reducing the stretch-to-draw ratio through increased clamping pressure enhances the deformability of uncured metal-CFRP laminates.

Conclusions

The flexural behaviour of the uncured metal-CFRP laminates is experimentally and numerically characterised by the analysis of load-displacement response, spring-back depth, length reduction and plastic strain in the clamped-beam bending process. The method is proposed under the condition of various clamping pressures on the local regions of the specimen and the factors affecting flexural behaviour, including material composition, layup and fibre orientation, processing temperature and clamping pressure are analysed in details. The relevant conclusions are:

(1) The application of clamping pressure has a significant impact on the flexural behaviour of the bent materials. With the increasing clamping pressure from 0 bar to 6 bar, the aluminium-based hybrid materials with a 2/1 layup decreases the interlaminar sliding length by 3%, resulting in a rise in plastic strain in the metal layer from 2.55% to 15.22% and a reduction in spring-back by 10%. It contributes to the result of a lower stretch-to-draw ratio and higher plastic deformation in uncured metal-CFRP laminates.
(2) The flexural behaviour of the uncured metal-CFRP laminates mainly depends on the metal composition and layup of the hybrid laminates. The aluminium-based laminates exhibit higher maximum bending force but greater spring-back after bending and unloading, while the stainless-steel based laminates undergo more plastic deformation and length reduction. The increasing of layup from 2/1 to 3/2 reduces the spring-back, and raises the bending force by slightly higher than the sum that of the corresponding single-layer metal sheets.
(3) The factors affecting the properties of CFRP material such as the fibre orientation and processing temperature play a limited role. The hybrid laminates with a fibre orientation of 45°/−45° have a slightly smaller maximum bending force than the same hybrid materials with a fibre orientation of 0°/90° at room temperature. The result differs in higher clamping pressure (6 bar) and higher temperature conditions (110°C) with a somewhat larger intra-ply shear force and inter-ply frictional force for the uncured CFRP material.
(4) The numerical simulation results show a good agreement with the experimental results at room temperature (23°C) with various clamping pressure for uncured metal-CFRP laminates. However, further validation is needed for temperature-dependent behaviours to refine interfacial friction models.

Author contributions

All authors contributed to the study conception and design. Material preparation, data collection and analysis were performed by Shichen Liu. The first draft of the manuscript was written by Shichen Liu and all authors commented on previous versions of the manuscript. All authors read and approved the final manuscript.

Declaration of conflicting interests

The authors declared no potential conflicts of interest with respect to the research, authorship, and/or publication of this article.

Funding

The authors disclosed receipt of the following financial support for the research, authorship, and/or publication of this article: The authors would like to thank the financial supports of China Scholarship Council (No. 201906040174).

ORCID iD

Shichen Liu https://orcid.org/0009-0002-2415-4699

Data Availability Statement

Data sharing not applicable to this article as no datasets were generated or analyzed during the current study.

References

1. Asundi A and Choi AYN. Fiber metal laminates: an advanced material for future aircraft. *J Mater Process Technol* 1997; 63(1-3): 384–394.
2. Sinke J. Manufacturing of GLARE parts and structures. *Appl Compos Mater* 2003; 10(4-5): 293–305.
3. Sinmazçelik T, Avcu E, Bora MÖ, et al. A review: fibre metal laminates, background, bonding types and applied test methods. *Mater Des* 2011; 32(7): 3671–3685.
4. Nardi D, Abouhamzeh M, Leonard R, et al. Investigation of kink induced defect in aluminium sheets for Glare manufacturing. *Compos Part A Appl Sci Manuf* 2019; 125(July): 105531.
5. Kavitha K, Vijayan R and Sathishkumar T. Fibre-metal laminates: a review of reinforcement and formability characteristics. *Mater Today Proc* 2020; 22: 601–605.
6. Olhan S, Antil B and Behera BK. Synergistic effect of different high-performance fibers on the microstructural evolution and mechanical performance of novel hybrid metal matrix composites produced via friction stir processing for

automotive applications. *J Engineering Manufacture* 2024; 239: 1–14.
7. Olhan S, Antil B and Behera B. Low-velocity impact and quasi-static post-impact compression analysis of woven structural composites for automotive: influence of fibre types and architectural structures. *Compos Struct* 2025; 352: 118676.
8. Mosse L, Compston P, Cantwell WJ, et al. The development of a finite element model for simulating the stamp forming of fibre-metal laminates. *Compos Struct* 2006; 75(1-4): 298–304.
9. Ding Z, Wang H, Luo J, et al. A review on forming technologies of fibre metal laminates. *Int J Lightweight Mater Manuf* 2021; 4(1): 110–126.
10. Heggemann T and Homberg W. Deep drawing of fiber metal laminates for automotive lightweight structures. *Compos Struct* 2019; 216: 53–57.
11. Chen Q, Boisse P, Park CH, et al. Intra/inter-ply shear behaviors of continuous fiber reinforced thermoplastic composites in thermoforming processes. *Compos Struct* 2011; 93(7): 1692–1703.
12. Erland S and Dodwell TJ. Quantifying inter- and intra-ply shear in the deformation of uncured composite laminates. *Adv Manuf Polym Compos Sci* 2021; 7(2): 25–35.
13. Liu S, Sinke J and Dransfeld C. An inter-ply friction model for thermoset based fibre metal laminate in a hot-pressing process. *Composites Part B* 2021; 227: 109400.
14. Liu S, Sinke J and Dransfeld C. A modified bias-extension test method for the characterisation of intra-ply shear deformability of hybrid metal-composite laminates. *Compos Struct* 2023; 314: 116964.
15. Liu S, Lang L, Sherkatghanad E, et al. Investigation into the fiber orientation effect on the formability of GLARE materials in the stamp forming process. *Appl Compos Mater* 2018; 25(2): 255–267.
16. Shichen L, Lihui L and Shiwei G. An investigation into the formability and processes of GLARE materials using hydro-bulging test. *Int J Precis Eng Manuf* 2019; 20(1): 121–128.
17. Liu C, Du D, Li H, et al. Interlaminar failure behavior of GLARE laminates under short-beam three-point-bending load. *Composites Part B* 2016; 97: 361–367.
18. Bellini C, Di Cocco V, Iacoviello F, et al. Performance evaluation of CFRP/Al fibre metal laminates with different structural characteristics. *Compos Struct* 2019; 225: 111117.
19. Zhao KM and Lee JK. Finite element analysis of the three-point bending of sheet metals. *J Mater Process Technol* 2002; 122(1): 6–11.
20. Seemuang N, Panich S and Slatter T. Bendability evaluation of sheet metals in three-point bending test by using acoustic emission features. *J App Sci* 2017; 16(2): 15–22.
21. Farrokhabadi A, Ahmad Taghizadeh S, Madadi H, et al. Experimental and numerical analysis of novel multi-layer sandwich panels under three point bending load. *Compos Struct* 2020; 250: 112631.
22. Mujika F. On the difference between flexural moduli obtained by three-point and four-point bending tests. *Polym Test* 2006; 25(2): 214–220.
23. Wang P, Hamila N and Boisse P. Thermoforming simulation of multilayer composites with continuous fibres and thermoplastic matrix. *Compos Part B* 2013; 52: 127–136.
24. Haanappel SP, Ten Thije RHW, Sachs U, et al. Formability analyses of uni-directional and textile reinforced thermoplastics. *Compos Part A Appl Sci Manuf* 2014; 56: 80–92.
25. Boisse P, Colmars J, Hamila N, et al. Bending and wrinkling of composite fiber preforms and prepregs. A review and new developments in the draping simulations. *Composites Part B* 2018; 141: 234–249.
26. Liang B, Chaudet P and Boisse P. Curvature determination in the bending test of continuous fibre reinforcements. *Strain* 2017; 53(1): 1–12.
27. Dörr D, Schirmaier FJ, Henning F, et al. A viscoelastic approach for modeling bending behavior in finite element forming simulation of continuously fiber reinforced composites. *Compos Part A Appl Sci Manuf* 2017; 94: 113–123.
28. Sachs U and Akkerman R. Viscoelastic bending model for continuous fiber-reinforced thermoplastic composites in melt. *Compos Part A Appl Sci Manuf* 2017; 100: 333–341.
29. Margossian A, Bel S and Hinterhoelzl R. Bending characterisation of a molten unidirectional carbon fibre reinforced thermoplastic composite using a Dynamic Mechanical Analysis system. *Compos Part A Appl Sci Manuf* 2015; 77: 154–163.
30. Ropers S, Kardos M and Osswald TA. A thermo-viscoelastic approach for the characterization and modeling of the bending behavior of thermoplastic composites. *Compos Part A Appl Sci Manuf* 2016; 90: 22–32.
31. Ostapiuk M, Bieniaś J and Surowska B. Analysis of the bending and failure of fiber metal laminates based on glass and carbon fibers. *Sci Eng Compos Mater* 2018; 25(6): 1095–1106.
32. Liu C, Du D, Li H, et al. Interlaminar failure behavior of GLARE laminates under short-beam three-point-bending load. *Compos Part B* 2016; 97: 361–367.
33. Li H, Xu Y, Hua X, et al. Bending failure mechanism and flexural properties of GLARE laminates with different stacking sequences. *Compos Struct* 2018; 187: 354–363.
34. Hu C, Sang L, Jiang K, et al. Experimental and numerical characterization of flexural properties and failure behavior of CFRP/Al laminates. *Compos Struct* 2022; 281: 115036.
35. SHD Composites. MTC510-UD epoxy prepreg datasheet. 2018; 01: 1–3. https://shdcomposites.com/admin/resources/datasheets/mtc510-tds-1.pdf
36. Desu RK, Nitin Krishnamurthy H, Balu A, et al. Mechanical properties of Austenitic Stainless-steel 304L and 316L at elevated temperatures. *J Mater Res Technol* 2016; 5(1): 13–20.
37. Santos AL, Nakazato RZ, Schmeer S, et al. Influence of anodization of aluminum 2024 T3 for application in

aluminum/Cf/ epoxy laminate. *Compos Part B* 2020; 184: 107718.

38. Keipour S and Gerdooei M. Spring-back behavior of fiber metal laminates in hat-shaped draw bending process: experimental and numerical evaluation. *Int J Adv Manuf Technol* 2019; 100(5-8): 1755–1765.
39. Sauvage JB, Aufray M, Jeandrau JP, et al. Using the 3-point bending method to study failure initiation in epoxide-aluminum joints. *Int J Adhesion Adhes* 2017; 75: 181–189.
40. Sharma T and Tyagi A. Review of mechanical modelling of fixed-fixed beams in RF MEMS switches. *Int Conf Adv Comput Commun Technol ACCT* 2013: 211–214.
41. Parsa MH, ahkamiEttehad SNM and Ettehad M. Experimental and finite element study on the spring-back of double curved aluminum /polypropylene/aluminum sandwich sheet. *Mater Des* 2010; 31(9): 4174–4183.
42. Wang J, Li J, Fu C, et al. Study on influencing factors of bending spring-back for metal fiber laminates. *Compos Struct* 2021; 261: 113558.